Samuel Frishman[1]
Mem. ASME
Department of Mechanical Engineering,
Stanford University,
Stanford, CA 94305
e-mail: samuel9@stanford.edu

Ali Kight[1]
Department of Bioengineering,
Stanford University,
Stanford, CA 94305
e-mail: akight@stanford.edu

Ileana Pirozzi[1]
Department of Bioengineering,
Stanford University,
Stanford, CA 94305
e-mail: ipirozzi@stanford.edu

Sainiteesh Maddineni
Department of Bioengineering,
Stanford University,
Stanford, CA 94305
e-mail: smaddineni@stanford.edu

Annabel M. Imbrie-Moore
Department of Mechanical Engineering,
Stanford University,
Stanford, CA 94305
e-mail: aimbrie@stanford.edu

Zulekha Karachiwalla
Department of Computer Engineering,
University of Maryland,
Baltimore, MD 21250
e-mail: zkarach1@umbc.edu

Michael J. Paulsen
Department of Cardiothoracic Surgery,
Stanford University,
Stanford, CA 94305
e-mail: mpaulsen@stanford.edu

Alexander D. Kaiser
ICME and Department of Pediatrics,
Stanford University,
Stanford, CA 94305
e-mail: alexdkaiser@stanford.edu

Y. Joseph Woo
Department of Cardiothoracic Surgery,
Stanford University,
Stanford, CA 94305
e-mail: joswoo@stanford.edu

Mark R. Cutkosky
Fellow ASME
Department of Mechanical Engineering,
Stanford University,
Stanford, CA 94305
e-mail: cutkosky@stanford.edu

DynaRing: A Patient-Specific Mitral Annuloplasty Ring With Selective Stiffness Segments

Annuloplasty ring choice and design are critical to the long-term efficacy of mitral valve (MV) repair. DynaRing is a selectively compliant annuloplasty ring composed of varying stiffness elastomer segments, a shape-set nitinol core, and a cross diameter filament. The ring provides sufficient stiffness to stabilize a diseased annulus while allowing physiological annular dynamics. Moreover, adjusting elastomer properties provides a mechanism for effectively tuning key MV metrics to specific patients. We evaluate the ring embedded in porcine valves with an ex-vivo left heart simulator and perform a 150 million cycle fatigue test via a custom oscillatory system. We present a patient-specific design approach for determining ring parameters using a finite element model optimization and patient MRI data. Ex-vivo experiment results demonstrate that motion of DynaRing closely matches literature values for healthy annuli. Findings from the patient-specific optimization establish DynaRing's ability to adjust the anterior–posterior and intercommissural diameters and saddle height by up to 8.8%, 5.6%, 19.8%, respectively, and match a wide range of patient data. [DOI: 10.1115/1.4054445]

[1]S. Frishman, A. Kight, and I. Pirozzi contributed equally to this work.

Manuscript received January 18, 2021; final manuscript received February 23, 2022; published online May 18, 2022. Assoc. Editor: Prasanna Hariharan.

1 Introduction

Mitral regurgitation (MR) remains the most common valvular abnormality and affects over 2% of the global population [1]. Myxomatous degeneration is the most prevalent etiology, characterized by the deterioration of the connective tissue that maintains the structural integrity of the mitral valve (MV) complex [2]. In particular, MR is often associated with the structural and functional disruption of the MV annulus, the ring of connective tissue bounding the mitral orifice that contributes to the effective and timely valve closure during systole and unimpeded filling of the left ventricle during diastole [3]. Thus, perturbations to the mechanical integrity of the MV complex give rise to mitral regurgitation, characterized by ineffective valve closure and consequent retrograde flow of blood from the left ventricle to the left atrium during systole.

In particular, mitral annular three-dimensional (3D) motion is thought to heavily contribute to valvular competency; specifically, a healthy annulus takes on a flat, dilated shape during diastole to enable filling and, through a sphincter motion, conforms to a saddle shape during systole to promote leaflet coaptation [4]. Furthermore, studies have elucidated the importance of these mitral annular dynamics on the uniform distribution of stresses across the MV complex, particularly the mitral leaflets [5]. Thus, MR treatment should focus on both restoring structural valvular geometry and the functional dynamics of the mitral annulus in order to promote long-term durability.

A common treatment for MR is MV repair, which often includes the implantation of an artificial annuloplasty ring to restore annular dimensions and proper leaflet coaptation with the aim of facilitating effective valve closure and mitigating retrograde blood flow [6]. However, studies have demonstrated that commercially available options unfavorably reduce annular dynamics and suggest the more rational design of annuloplasty rings using concepts of functionally graded materials for heterogeneous support [7]. Our prior work introduced DynaRing, a selectively compliant annuloplasty ring of varying stiffness that aims to restore annular dimensions while enabling critical annular dynamics (Fig. 1) [8].

Patient variability remains an important factor in MV treatment longevity [9]; however, the span of current rings on the market fails to encompass the variations in dynamic annular geometry and pathology across patients. Several groups have demonstrated the ability for automated, rapid imaging of patient annuli through techniques such as 3D echocardiography and cine MRI, motivating the transition toward tailored ring design based on patient imaging data [10,11]. In particular, Sündermaan et al. demonstrated the feasibility of patient-specific annuloplasty ring design, wherein a customized, solid metal ring was constructed from electrocardiogram gated-CT imaging in pigs [12].

Inspired by the need for patient specificity, we expand on our previous work on the development of a selectively compliant annuloplasty ring by (1) investigating a modular ring design process (Fig. 2) that is informed by patient data and (2) evaluating the long-term durability of the patient-specific ring using fatigue testing.

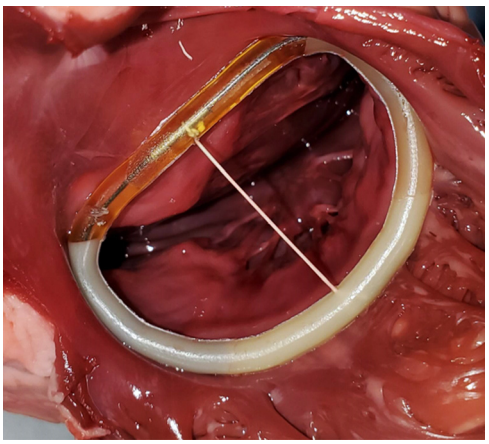

Fig. 1 DynaRing is a selectively compliant annuloplasty ring. A shape-set NiTi wire is embedded in four elastomer segments of varying stiffness and an AP mounted filament controls the AP diameter.

2 Related Work

New insights into the 3D dynamic behavior of the mitral valve and the necessity to homogenize tissue mechanics have prompted a reevaluation of annuloplasty ring designs. For example, Purser et al. suggest the use of a shape-memory core, which resulted in reduced deformation of surrounding tissue compared to commercial semirigid rings [13]. In pursuit of a similar objective, Tjørnild et al. use 3D printing to vary ring geometry and control the ring properties [14].

Furthermore, recent studies have evaluated the use of soft polymers to promote annular dynamics following ring implantation. In a recent study, Pierce et al. develop a flexible ring through fast-setting silicone with a shore hardness of 40A [15]. Implantation of the flexible ring with multiple force transducers enabled a comparative analysis of cyclic dynamic forces in healthy Dorsett hybrid sheep. The results demonstrated that the lower stiffness ring preferentially reduced suture forces on the structurally weaker posterior annulus as compared to rigid and semirigid rigs, motivating stiffness as a parameter to vary when optimizing potential annuloplasty ring designs. In order to demonstrate the feasibility of a multimaterial ring design that enables annular dynamics while also providing structural integrity, Ncho et al. demonstrated the development of a heterogeneous annuloplasty ring using a combination of titanium and silicone segments [16].

The insights gained from prior investigations on annuloplasty ring designs motivate the combination of mechanical heterogeneity and multimaterial design to achieve optimized ring dynamics and structural support. In this work, we expand on previous efforts by providing a modular, selectively compliant ring design and method for optimizing segment stiffnesses to match patient-specific parameters.

3 Ring Design

Healthy annular motion is critical to the long term efficacy of mitral valve repair. While annular dynamics vary greatly among

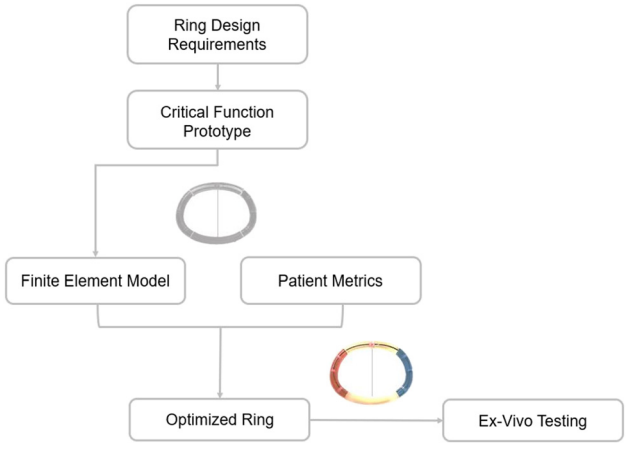

Fig. 2 Annuloplasty ring design flowchart. A critical function prototype is developed from initial design requirements using variable stiffness segments over a nitinol core [8]. A representative finite element model is constructed and segment stiffnesses are optimized to match desired patient metrics. The optimized ring is then fabricated and tested in an ex-vivo setup.

patients [10], today's commercially available rings fall into broad categories based on patient size, overall rigidity, and initial conformation. An ideal ring includes readily adjustable features that are tailored to specific patients based on disease state and patient anatomy. The following design requirements guide our approach to a patient-specific annuloplasty ring. Specifically, the design must have the ability to

- vary initial ring conformation
- change stiffness values along ring perimeter
- control variation in anterior–posterior (AP) diameter
- undergo approximately 800 million cycles (20 years)

To achieve these criteria, we utilize a shape-set, super elastic Nitinol (NiTi) wire core embedded in polymer segments of varying stiffness and an AP-mounted filament. Shape-setting properties of the NiTi core enable matching the initial conformation of the ring to specific patients. Moreover, the NiTi core provides structural rigidity to contract a dilated valve and promotes ring longevity. The polymer segments, cast around the NiTi core, provide ability to specify bending stiffness along the ring perimeter and greatly influence dynamic properties of the mitral annulus. The AP-mounted filament provides direct control of AP diameter and passively induces saddle shape formation. Choice of elasticity in the filament dictates AP diameter variation throughout the cardiac cycle and controlling AP diameter has been shown to significantly impact leaflet coaptation in MR [17].

Four segments in DynaRing mimic the four primary morphologies of the MV: anterior, posterior, commissural left (Cl), commissural right (Cr). Stiffness values of each segment dictate annular motion and resulting functional metrics such as orifice area and saddle height. In Sec. 4.1, we describe an optimization technique that leverages patient data to determine desired stiffness values for each segment. To evaluate DynaRing's annular dynamics in an ex-vivo experiment, we created a prototype using the manufacturing process described in our previous work [8]. We provide a summary of the manufacturing process below (Fig. 3). Polymers were selected to match tissue properties found in Ref. [18] with segments preserving the relative stiffness (ratio of Young's moduli) between annulus sections. The materials selected for the physical prototype were smooth-on room temperature vulcanizing urethanes PMC 70A, Vytaflex 30A, Vytaflex 40A, and Vytaflex 50A for the anterior, posterior, Cl, and Cr, respectively. Room temperature vulcanizing urethane provides an effective prototyping material, however, in future designs, other polymers will be used to ensure biocompatibility.

3.1 Manufacturing. DynaRing is manufactured with two main processes: (A) NiTi shape setting, (B) polymer segment casting (Fig. 3). NiTi is selected for its biocompatibility, fatigue resistance, and shape memory properties. The NiTi wire used is 0.38 mm in diameter (Malin Co. Gauge.015). A 112 mm long piece is shape set using a Joule heating method described in Ref. [19]. The wire is placed into a 3D printed mold and secured with screws that form leads to the Joule heating circuit. The mold shape is similar to the 3D conformation of the Physio-II 40 ring. Beads are glued at specific points on the wire (inset Fig. 3) and are used for alignment in the casting process. The ends of the shape-set NiTi wire are connected with a thin metal sleeve to complete the core. Finally, prior to casting, a polytetrafluoroethylene (PTFE) filament is tied across the AP diameter.

Polymer casting occurs in two steps with the anterior and posterior segments cast first, followed by the left and right commissures. The commissure segments are cast prior to full cure of the anterior and posterior to ensure a strong bond between ring segments. Alignment beads, secured to the NiTi wire earlier in the process, are used to position the core in the mold.

4 Design Methods

4.1 Patient-Specific Optimization. The modular design of DynaRing allows for tuning of segment stiffnesses to achieve the desired functionality. In clinical practice, ideal ring functionality could be determined through a combination of patient imaging and degree of MV annular dysfunction [9]. Here, as a proof of concept, we demonstrate the tunability of DynaRing by optimizing segment stiffnesses to achieve various dynamic trajectories of healthy annuli, as defined by changes in functional metrics of saddle height (SH), anterior–posterior (AP) diameter, and

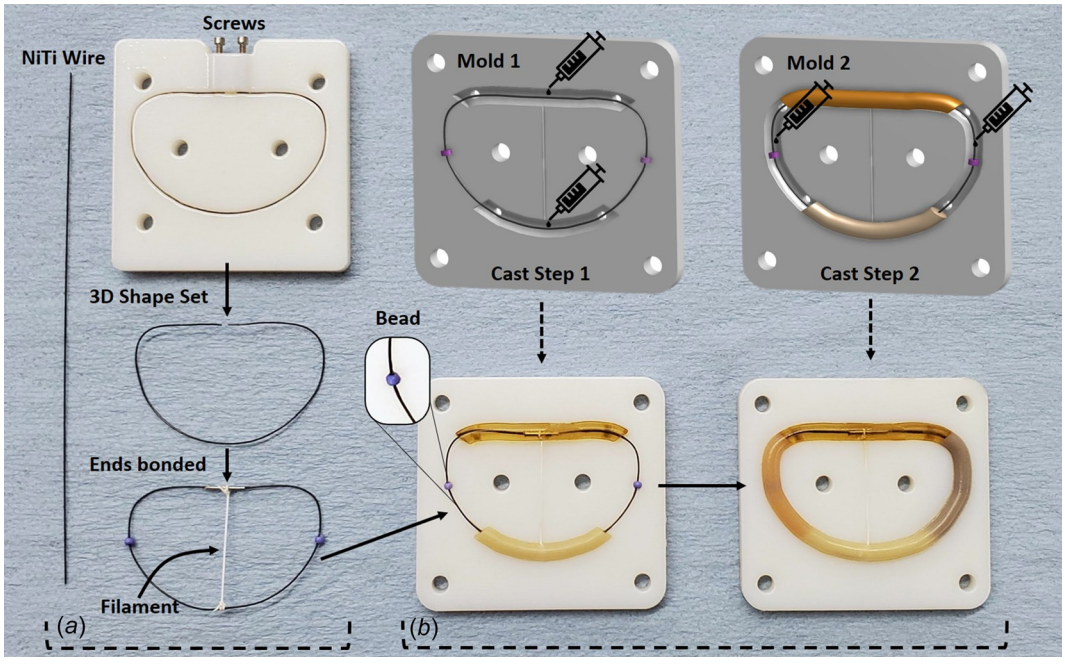

Fig. 3 Manufacturing process. (*a*) An NiTi wire is shape set into a 3D conformation and the wire ends are connected with a thin metal sleeve. A filament is mounted between the AP diameter. (*b*) Individual polymer segments are cast by injecting material into an enclosed mold (only half the mold is shown in the image).

Table 1 Range of metrics achievable by varying DynaRing segment stiffness values between 0.01 MPa to 100,000 MPa

	SH	AP	IC
Min (%)	2.9	0.0	0.1
Max (%)	19.8	8.8	5.6

intercommissural (IC) distance [20]. Considerations for implementation in a clinical setting where a patient's predisease MRI data are not available are detailed in the Optimization and Discussion sections. The AP diameter was defined as the 3D distance between the midpoints of the anterior and posterior segments. Similarly, the IC diameter was defined as the 3D distance between the midpoints of the left and right commissural segments. Finally, the saddle height was selected as a measure of annulus flexion during the cardiac cycle, and was defined as the vertical distance between the highest and lowest points on the annulus.

The advancement of finite element (FE) modeling methods provides an efficient platform for in-silico device optimization and has demonstrated efficacy in assessing the biomechanical effects of mitral valve repair and annuloplasty ring design [21]. Nevertheless, optimization with FE models can become computationally expensive and time-consuming when searching over a multidimensional design space, such as the one presented here. Moreover, the lack of an explicit representative analytical expression prohibits the use of gradient-based optimization. In this case, the use of Bayesian Optimization through a surrogate model provides a derivative-free, efficient alternative [22]. A Gaussian Process Regression with a Matérn kernel was chosen to formulate the surrogate model given that the degree of uncertainty for any design point can be explicitly calculated. An expected improvement exploration acquisition function was iteratively employed for parameter optimization [23–25]. All optimization algorithms were written and implemented in Python (code available upon request). The construction of the FE model is detailed in Sec. 4.3.

MRI annular tracking data from healthy individuals was obtained from Ref. [11]. Based on this data, we identified a range of variability in metrics representing annular dynamics. Specifically, each subject's annular motion was characterized through change in saddle height, AP Diameter, and IC distance for a single cardiac cycle. Here, the optimization process is demonstrated for the cases of two simulated patients, patient A and patient B. A and B were selected to demonstrate a significant difference in annular dynamics in an effort to illustrate the power of the design and optimization to achieve metrics across the physiological spectrum. Additional optimization parameters, such as filament elasticity and pretension, may be included in future iterations to better enable independent control of metrics and reduce coupling. The surrogate model was developed using fifty training data points obtained through FE simulations of the ring with variable segment stiffnesses, as defined by a Latin hypercube sampling of the four-dimensional design space (ranging from 0.01 MPa to 100,000 MPa) [23]. The cost function, $J(x)$, was defined as the difference between FE simulated functional metrics and ideal patient metrics (Eq. (1))

$$J(x) = (\mathrm{AP} - \mathrm{AP}(\mathbf{x})^*)^2 + (\mathrm{IC} - \mathrm{IC}(\mathbf{x})^*)^2 + (\mathrm{SH} - \mathrm{SH}(\mathbf{x})^*)^2 \quad (1)$$

where AP, IC, and SH represent AP diameter, IC distance, and saddle height ideal metrics, respectively, and $AP(x)^*$, $IC(x)^*$, and $SH(x)^*$ represent the simulated metrics for a given state of segment stiffnesses, x. Thus, the optimization of the surrogate model with respect to $J(x)$ results in the DynaRing segment stiffnesses that achieve the ideal metrics under physiological loading conditions. Investigations into annular dynamics for various MR etiologies have demonstrated a significant deviation of all three metrics in the disease state compared to healthy controls [26,27]. For these reasons, the cost function was constructed as a sum of equally weighted metrics. Future work includes investigation on the relative importance of individual metrics. Optimizing for known ideal ratios, such as maintaining an AP:IC ratio of 3:4 and an annular height to commissural width ratio of greater than 15%, is an alternate approach for clinical settings where healthy baseline MRI data are not available [27].

Table 1 summarizes the maximum and minimum percentage changes observed in a Latin hypercube sample of 50 different stiffness combinations that were evaluated in our FE model. Details on the FE model are described in Sec 4.3.

Prior to the patient optimization, an intuitive test case was run to validate the proposed optimization pipeline. For the test case, all target metrics were set to 0% change (i.e., an immobile annulus) with expected convergence at high stiffness for all segments in order to prevent motion (upper bound Young's modulus (YM) of 100,000 MPa). Figure 4 displays the results of these validation tests. First, only the anterior segment was optimized, and the posterior, left, and right segments were set to a constant of 100,000 MPa (Fig. 4(*b*)). This test resulted in anterior segment stiffness of 100,000 MPa, as expected. Then, a two-dimensional test was performed with both the anterior and posterior segments' stiffness optimized while the left and right segments were held constant at 100,000 MPa. Finally, all four segments were allowed to vary in a final validation test. The expected improvement model converged to an optimal design of all four segments having an YM of 100,000 MPa, as predicted.

4.2 Ex-Vivo Experimental Setup. To investigate DynaRing's ability to enable annular dynamics, we performed ex-vivo experiments in the Stanford left heart simulator (LHS) [28,29] with porcine valves. The simulator is actuated with a ViVitro pump and includes a junction between the atrial and ventricular chambers that acts as the location of the mitral valve (Fig. 5). Details can be found in our previous work [8]; a summary is provided here. Two primary rings were tested under analogous conditions: our custom DynaRing and a physio-II ring (an example commercially available semirigid ring). For mounting inside the heart simulator, rings were embedded inside a soft silicone sewing cuff (smooth-on dragon skin 20A), which forms a seal between the chambers. A healthy porcine valve was excised to include the mitral valve, surrounding annular tissue, and the papillary muscles connected via the chordae tendineae. The annuloplasty ring and sewing cuff were then sutured to the porcine valve and secured in the LHS junction between the atrial and ventricular chambers (Fig. 5). Finally, the papillary mounts were connected to the bottom of the ventricular chamber.

Custom microcoordinate markers and a dual-camera system were used to track annular motion (Sony Cyber-shot DSC-RX0 II, Sony, New York). The coordinate markers (inset Fig. 5(*c*)) were 3D printed (Form2 rigid) and colored at the origin and each end point. The markers provide 6DoF information on the vector normal to the plane of the annulus surface. Given the perpendicular axes constraint between coordinate points, a least-squares optimization via Procrustes analysis was used to improve 3D reconstruction accuracy [30].

For each test, twelve markers were pinned to the ring using a needle tip embedded into the 3D printed part. The cameras were calibrated using a jig with known marker positions. The LHS was run at physiological pressures and flows and high frame rate (480 fps) video was captured over four cardiac cycles. Marker motion was then determined from the videos using direct linear transform software for biological and biomimetic applications [31].

4.3 Modeling. A FE model of DynaRing embedded in a silicone sewing cuff was constructed in SOLIDWORKS (Solidworks, Mathworks) (Fig. 6). A fixed boundary condition was applied

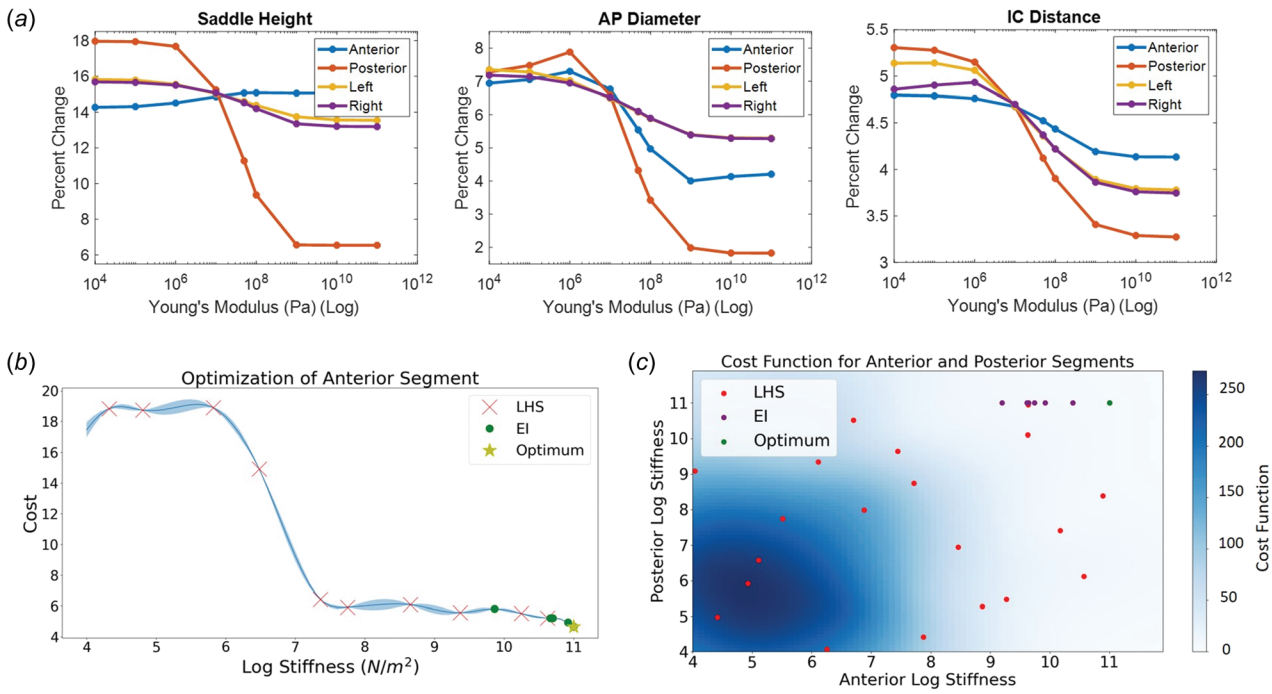

Fig. 4 Validation of the Bayesian optimization with all goal metrics set to 0% change. (*a*) Sensitivity analysis of each segment for each metric. (*b*) Optimization of only the anterior segment holding the remaining segments at maximal stiffness. (*c*) Optimization of anterior and posterior segment holding the left and right segments at maximal stiffness.

along the circumferential face of the sewing cuff, representing fixation to the LHS. Net pressures, extracted from pressure measurements in the LHS, of 140 mmHg and −4 mmHg were applied to the inferior (ventricular) face of the sewing cuff to replicate systole and diastole, respectively. Strain in the systolic configuration is shown in Fig. 6(*a*). A linear isotropic material with tetrahedral elements was used; additional details on the FE model, including material properties, can be found in our previous work [8]. Although not representative of the nonlinear nature of the polymeric design, a linear approximation was assumed adequate to demonstrate trends associated with segment stiffness modification. As an improvement to the original model, the PTFE, cross-diameter filament was simulated via application of 1 N forces on the anterior and posterior segments pointing to the interior of the DynaRing (chosen to be similar to chordal forces found in Ref. [32]). Depending on the fiber material and pretension, different modeling techniques could be employed. To better understand how sensitive the optimization results are to the PTFE line and its attachment, we compared the constant force to a spring connector element and resultant performance metrics were within 1% for a spring generating forces centered at 1 N. Finally, mitral leaflet forces were applied to the model based on prior modeling

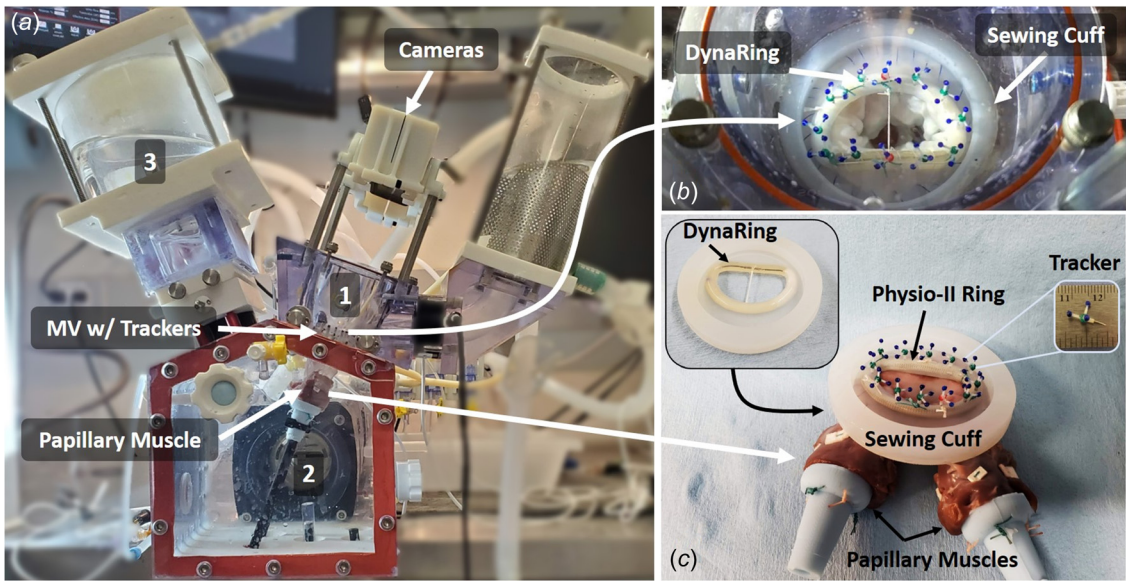

Fig. 5 (*a*) Left heart simulator. The device includes (1) atrial, (2) ventricular and (3) aortic chambers. A ViVitro pump cycles fluid at physiological flow rates and pressures. (*b*) A camera view of the DynaRing mounted inside the simulator with tracking markers embedded. (*c*) The sewing cuff, with an embedded annuloplasty ring, mounted to a porcine valve.

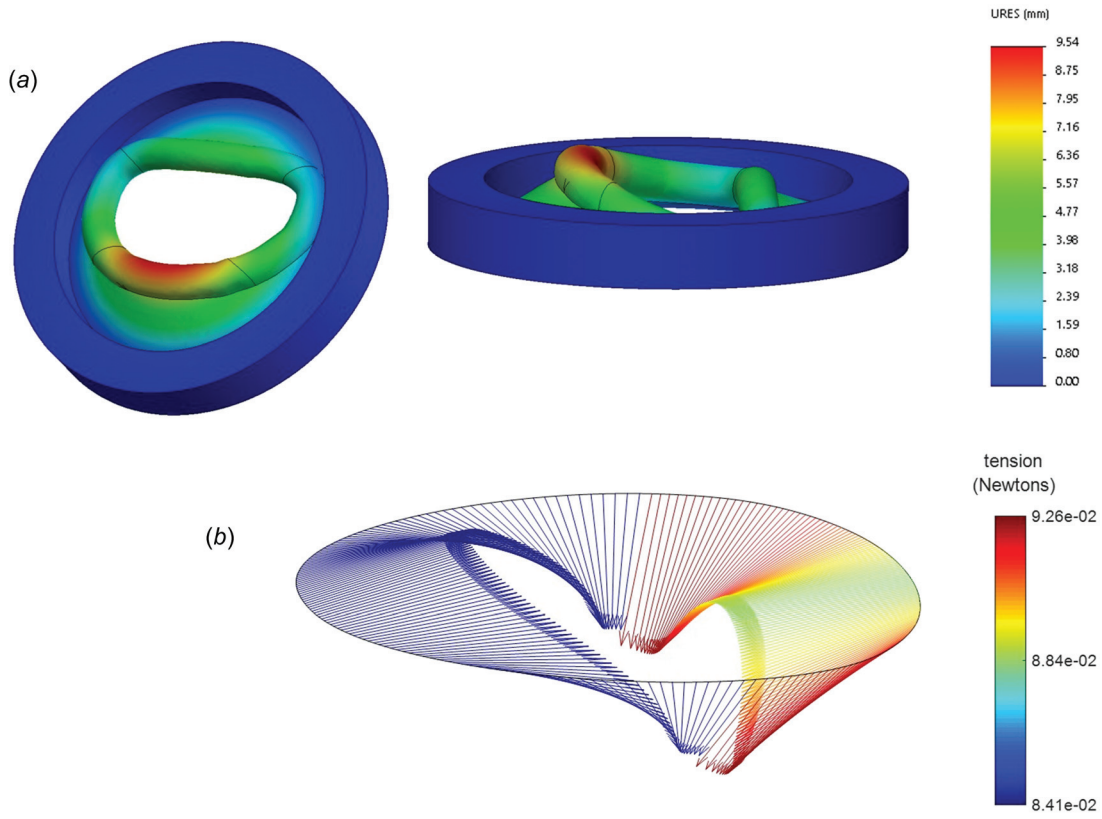

Fig. 6 (*a*) Strain results from the finite element model and (*b*) annular forces applied in addition to atrial and ventricular pressures on the model faces

and simulation of the mitral valve that incorporates leaflet and chordae tendinae mechanics [33]. Specifically, the model used in Ref. [33] was modified such that the annular geometry matched DynaRing geometry. A mechanical equilibrium was solved for at systolic pressure, and net forces on the annulus were extracted, shown in Fig. 6(*b*). For more detail on the numerical methods involved, we refer to previous work by our collaborators [33]. The extracted forces were then summed into net forces per DynaRing segment and applied to the DynaRing FE model. Percent change between maximum and minimum pressure combinations experienced in the LHS for each functional metric (AP diameter, IC distance, and saddle height) were evaluated for patient-specific optimization.

4.4 Fatigue Testing. The average mitral valve undergoes roughly 700k cycles per week. To ensure ring longevity, and in particular durability of DynaRing segment bonds, we performed a 150 million cycle fatigue test using a custom device (Fig. 7). The device consists of a slider-crank mechanism with a DC motor driving the crank. The slider stroke length is 1 cm, chosen to induce an upper bound deflection to those expected in vivo [11], and is fixed to the ring with a link across the AP diameter. As the motor rotates, the ring flexes back and forth, mimicking saddle formation during a cardiac cycle. The motor rotates at 3000 rpm, resulting in a 50 Hz oscillation of the ring. The force to deflect the ring 5 mm was measured using a mark-10 force gage approximately every 35 million cycles. Additionally, segment joints were visually inspected for delamination.

5 Results

5.1 Ex-Vivo

5.1.1 Evaluation Metrics. To characterize annular dynamics, four commonly reported metrics used to define MV geometry were chosen for ease of comparison: (1) AP diameter, (2) IC distance, and (3) saddle height, and (4) mitral orifice area [20]. Metrics (1)–(3) were calculated as described in the Patient-Specific Optimization section, where midpoints were defined with annular markers. To calculate the orifice area, the twelve annular markers and their geometric centroid were used to divide the annulus into

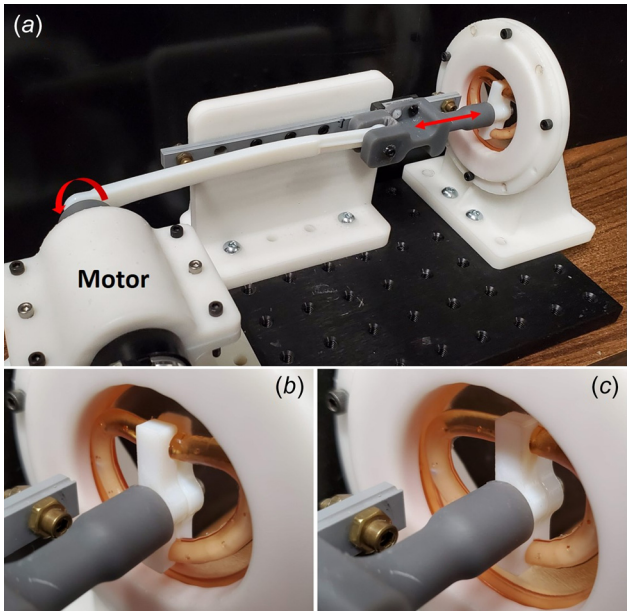

Fig. 7 (*a*) A custom oscillatory device for fatigue testing the annuloplasty ring. A motor drives a crank slider mechanism to oscillate the ring at 50 Hz over a 1 cm stroke. (*b*) Bottom of the stroke, and (*c*) top of the stroke.

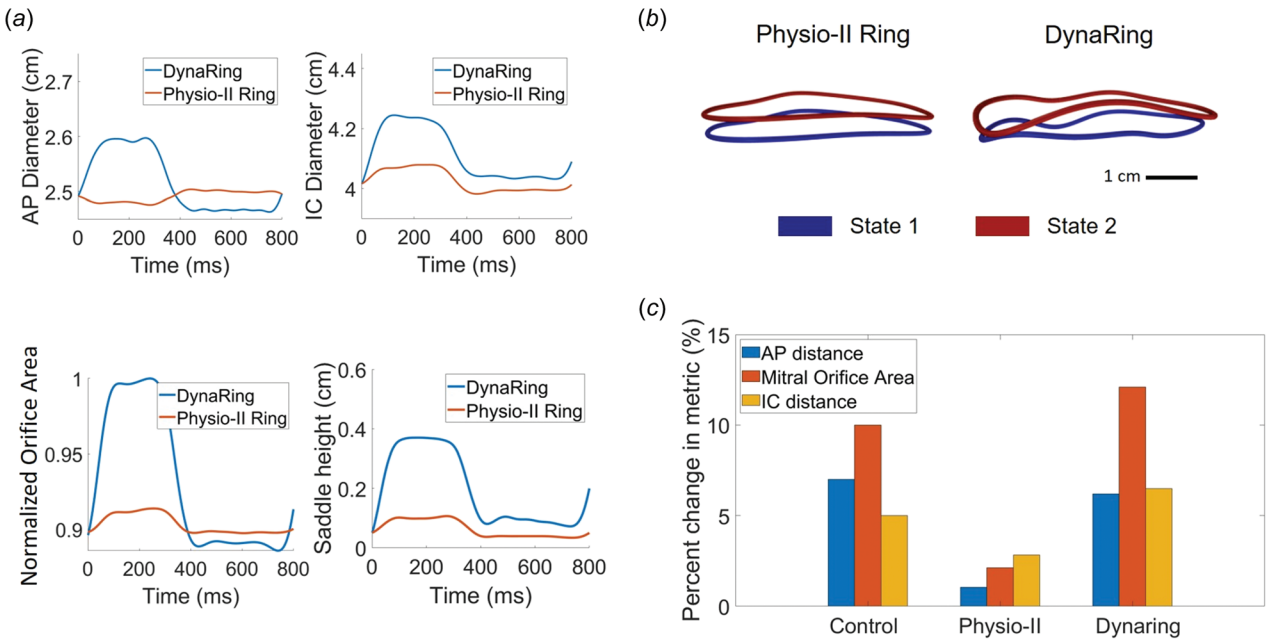

Fig. 8 (*a*) Tracking data over the cardiac cycle for each metric. (*b*) Ring conformations at respective maximum and minimum locations. (*c*) Metric comparison between the two rings and literature control values.

12 triangular regions. The area was then calculated as the sum of the areas of all the regions.

5.1.2 Comparative Performance. Figure 8(*a*) shows the various metric changes tracked over a single cardiac cycle for two cases: physio-II and DynaRing. Orifice area and AP distance change dynamically from late diastolic maxima to early systolic minima for the DynaRing case (with percent changes of and 12% and 6%, respectively), whereas the Physio-II Ring case features a minimally varying orifice area and AP distance throughout the cycle (1% and 2% changes, respectively). For IC diameter and saddle height, both cases follow a similar pattern throughout the cycle, with DynaRing showing a much greater maximum variation over the cycle compared to physio-II. A time-series visualization of annular performance metrics for a healthy human control, comparable to patients A and B, can be found in Ref. [11].

Figure 8(*b*) shows reconstructed 3D annular conformations at two selected states in the cycle: state 1 (representative of diastole) and state 2 (representative of systole) for the physio-II and DynaRing cases. The semirigid Physio-II ring at both stages of the cardiac

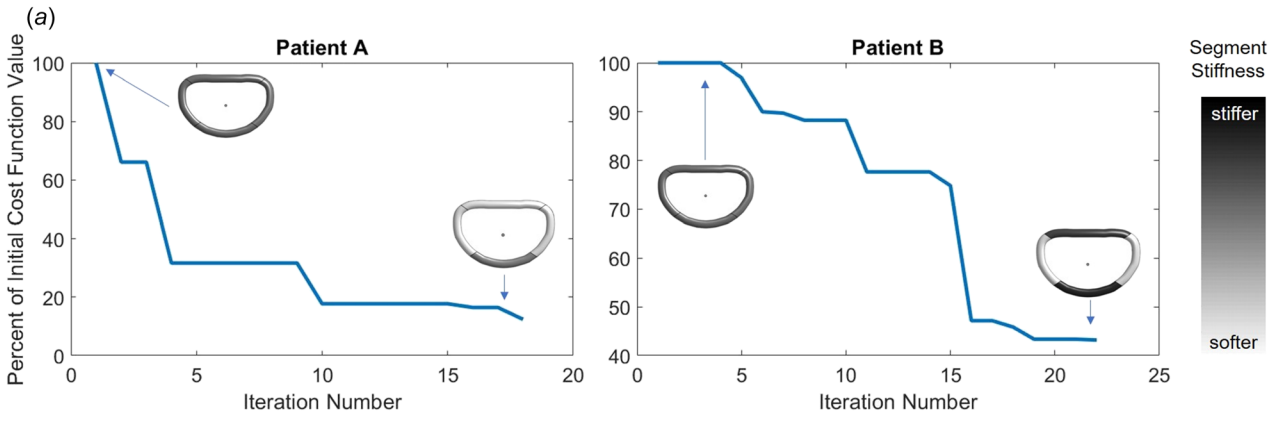

(*b*)

Metric	Mock Patient A			Mock Patient B		
	Target (%)	Actual (%)	% Error	Target (%)	Actual (%)	% Error
AP Diameter	6.8	5.43	19.6	1.0	1.13	12.9
IC Distance	4	4.64	14.8	2.0	1.86	7.1
Saddle Height	8.5	8.76	3.5	4.5	4.59	2

Fig. 9 (*a*) Optimization results for patients A and B. The plots present the best candidate at any given iteration and display schematics of the initial and final ring stiffnesses. (*b*) Final metric values summarized.

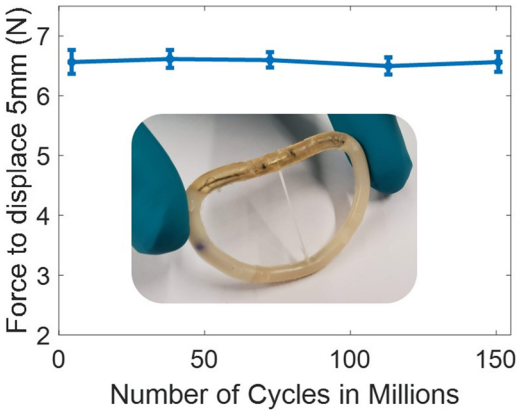

Fig. 10 The force to flex the ring 5 mm measured at intervals of roughly 35 million cycles. The inset includes an image of the ring extracted from the sewing cuff at over 100 million cycles. No visible damage on the segment joints was observed.

cycle demonstrates virtually no change in 3D conformation. In contrast, DynaRing's conformational change displays desired changes in area as well as a saddle-shaped 3D conformation.

In Fig. 8(*c*), we compare the metrics of the ring test cases to literature control values obtained via in vivo cinefluoroscopy in sheep, using the same metrics as those described in this study [20]. A time-series representation of this control data can be found in Ref. [20]. Control metrics for AP diameter, IC diameter, and orifice area were closest to the performance metrics reported for DynaRing. Specifically, the three aforementioned metrics, compared between DynaRing and control, are as follows: AP diameter 5.4±0.3% versus 7±1%; IC diameter 6.6±1.3% versus 5±1%; orifice area 12.5±3% versus 10±2%. With respect to all performance metrics, the commercial physio-II ring and the reported literature values for healthy control differ significantly ($p < 0.001$), and significant differences between physio-II and DynaRing ($p < 0.001$) were also demonstrated. Furthermore, DynaRing preserves the natural 3:4 ratio between the AP and IC diameter during systole, while the physio-II ring demonstrates a ratio of 2:3 [11].

5.2 Optimization. To evaluate the patient-specific tunability of DynaRing, Bayesian Optimization via a Gaussian Process surrogate model was performed on two simulated patients' data. The optimization function was run over 25 iterations, with the stiffness combination associated with the lowest predicted cost function in the surrogate model chosen for iterative evaluation by the FE model. Figure 9 shows the results of optimization for two patients. The minimum cost function observed during optimization was plotted, with diagrams illustrating the evolution of DynaRing's design until an optimal solution was found. Cost function is plotted as a percentage of the cost associated with the lowest cost sample from Latin hypercube sampling.

For patient A, larger percentage changes in mitral valve metrics were chosen: AP diameter 6.8%; IC diameter 4.0%; saddle height 8.5%. A 56% decrease in cost function was observed in the optimal DynaRing design compared to the initial optimum in the Latin hypercube sample. The optimization converged to a final design with YM of 0.01 MPa in the anterior, left and right segments, and a stiff posterior segment with YM of 149 MPa. The percent deviation of the final design's change in mitral valve metrics compared to the target inputs are as follows: AP diameter 19.7%; IC diameter 14.8%; saddle height 3.5%.

In order to evaluate how differing target metrics can change DynaRing design optimization, the target changes in mitral valve metrics for patient B were smaller than those for patient A: AP diameter 1.0%; IC diameter 2.0%; SH 4.5%. This time, a 93.2% reduction in cost function was observed in the optimal DynaRing compared to the best design from the Latin hypercube sample, indicating substantially more optimization occurred with smaller target metrics. The optimization converged to a final design with following YM values: anterior 1720 MPa; posterior 1960 MPa; left 58.1 MPa; right 120 MPa. As expected, the segments were stiffer on average with patient B compared to patient A. Finally, the percent deviation of the final design's change in mitral valve metrics compared to the target inputs are as follows: AP diameter 12.9%; IC diameter 7.1%; SH 2.0%.

5.3 Fatigue. Figure 10 presents force data gathered throughout the fatigue test and an image of the ring after over 100 million cycles. At roughly 35 million cycle intervals, the oscillatory device was paused, and the force to deflect the ring 5 mm was measured. Forces were applied parallel to the linear rail at the center point of the AP mounted link (Fig. 7). No statistically significant force deviation is present over the cycles and the segment bonds remained intact based on visual inspection.

6 Discussion

In this study, we expand on our previously reported design of DynaRing, a selectively compliant annuloplasty ring of variable stiffness aimed at restoring annular geometry while enabling dynamic motion [8]. This work addresses the critical need to develop an annuloplasty ring with superior dynamic performance compared to commercially available semirigid rings. Patient-specific design has been described as a major trend expected to revolutionize medicine in the next decade [34]. In the context of annular dynamics, our studies show that a patient-specific approach is highly desired due to the greatly variable nature of interpersonal annular dynamics, even in healthy individuals, as demonstrated by Ref. [11]. Here, we propose a patient-specific design pipeline for annuloplasty rings and demonstrate its utility in determining ideal segment stiffness based on individual subjects' annular motion. Overall, our experimental results demonstrate a design process to achieve predetermined subject-specific annular motion through appropriate segment stiffness selection enhanced by a custom Bayesian optimization approach. Given the demanding loading conditions involved in mitral valve mechanics, a major concern is the durability and integrity of the materials employed in the fabrication of the ring. Our mechanical 150 M cycle fatigue testing demonstrated DynaRing's material and design integrity through force-measurements and visual inspection. In relation to the ISO 5910 cardiovascular implants standards, our fatigue test addresses the primary physiological loading experienced by the ring, specifically bending. Additional testing is needed to examine other loading modes including radial dilation and compression. Moreover, careful control of temperature is required by the ISO 5910 standard and will be implemented in subsequent fatigue tests with the final biocompatible polymers.

The dynamic behavior of the physical prototype was evaluated in our in-house left heart simulator to track dynamic performance and enable comparative analysis with literature controls as well as commercially available alternatives. As previously reported, DynaRing dynamic behavior closely matches literature control metrics for change in AP and IC diameter, orifice area and SH (Fig. 8). In contrast, the commercial semirigid ring alternative exhibits minimal variation in shape and prohibits the formation of an annular saddle, whereas DynaRing achieves a 3× increase in SH.

To address the high variability in subject-specific dynamic behavior, we propose the use of a patient-specific optimization pipeline used to demonstrate that selective stiffness of DynaRing segments is an effective method for tuning annular metrics to specific patients (Fig. 9). The simulated patients' data reported here, based on metrics derived from MRI tracking data, display significant differences in target metrics. In both instances, the optimization converges to a suitable combination of stiffness values, which is tailored to each subject. Of the metrics, AP diameter exhibits largest variation in target values (19.6% and 12.9% for patient A and B, respectively). The metrics selected to characterize dynamic behavior are inspired by the rich literature describing annular

dynamics. Nevertheless, despite having selected widely reported metrics of annular function, such parameters display some mechanical coupling, particularly between AP and IC diameter. This observed behavior limits the theoretically achievable combinations compared to if the metrics were idealized as independent variables. In future work, filament material and pretension, as additional optimization parameters would provide a means for finer and more independent adjustment of AP diameter. A filament connecting the left and right commissures may also be tested to more directly control IC diameter variation. Moreover, initial ring conformation may be considered to match patient specific shapes. Each parameter, however, has implications for integration into a clinical practice. For example, polymer casting can be readily conducted at a clinic with a small, automated machine. Variation in ring conformation, however, requires different shape set nitinol cores and is a more intensive manufacturing step.

In the Bayesian optimization process we propose, predictions are made on the annulus' dynamic behavior based on the FE model we developed from experimental data. In our previous report, we determined consistent results between experimental testing and FE simulation, despite an over-prediction of orifice area by the FE model. In this study, we corrected the aforementioned shortcoming by accounting for the effect of forces from the leaflets via the chordae tendineae acting on the mitral annulus, which constrain and affect its motion. Inclusion of such forces in this work significantly improved its predictive power. Although it remains an open question how closely the parameters must match to be acceptable in practice, we observed significant improvement in orifice area prediction with our new model as compared to previous work [8].

Preliminary fatigue testing (150 million cycles) provides confidence in the segmented polymer design of DynaRing. Mating features at the segment bonds can be added for additional bond integrity. Further ring iterations will include a fabric sheath that encases the ring to further ensure cohesion of ring elements. Additional fatigue testing will be required once final polymer materials are selected and will be conducted in accordance to the ISO 5910 standards.

6.1 Study Limitations and Future Work. In this study, the primary goal was to validate the concept and application of a patient-specific optimization pipeline. Thus, optimization target values were determined from MRI data collected from healthy individuals. While this approach provides a means to validate the concept of optimal selection of segment stiffness based on individual-specific target metrics, the clinical applicability of these results is limited by the lack of pre-existing valvular pathology in the cases analyzed. Specifically, experimental data were collected from healthy porcine valves and 3D annular tracking data refers to healthy individuals. This limitation is partially due to the lack of high-fidelity disease models for regurgitant mitral annuli. In parallel work [35], our collaborators developed a 3D-printed device to simulate and produce pathophysiologic mitral annular dilation in a diseased valve. The method proposed by Imbrie-Moore et al. could thus be used to reproduce more accurate pathological physiology.

In future work, the process proposed here can be integrated in the clinical workflow of data collection for diseased patients. In a clinical workflow of a diseased case, imaging methods in combination with physician expertise could define desired annuloplasty ring function and resulting target parameters. We note that the current FEA model omits native annular tissue and assumes properties of the annuloplasty ring dominate the system. Improved models that include stiffness provided by the native annulus would further enhance the predictive ability of our ring design process. Further, chordal and leaflet forces input into the FE model could be more representative of the patient's disease state by modifying the model in Ref. [33] to simulate patient-specific diseased annular geometry derived from imaging.

In addition to the fatigue test limitations described in the discussion with respect to the ISO 5910 standards, we note that experiments described in this work were performed on a small number of DynaRing prototypes. Additional testing is needed to understand variability in the manufacturing process and its impact on the LHS experiments. Future testing will be performed in beating heart models such as those described in Refs. [36] and [37] and can include comparison to rigid and flexible rings.

Lastly, future work includes investigation of transcatheter deployment. DynaRing's NiTi core and polymer segments enable substantial deformation, potentially allowing for a ring design that collapses into a sufficiently small form factor for delivery through a catheter.

7 Conclusion

We present a selectively compliant annuloplasty ring for enabling patient-specific annular motion. Our ex-vivo studies demonstrate DynaRing's ability to achieve healthy annular motions and outperform commercial semirigid rings. Moreover, the patient-specific optimization method illustrates a design process for tailoring ring parameters to patient data by varying segment stiffnesses. We perform the optimization on two simulated patients, based on real MRI data, that include significantly different valve metrics and achieve suitable ring designs in each case. Finally, we demonstrate the feasibility of a segmented polymer ring design with a 150 million cycle fatigue test.

Acknowledgment

This work is funded in part by the National Science Foundation (GRFP), the National Institute of Health (5R01HL152155-02), the American Heart Association, the National Heart, Lung and Blood Institute, and the Knight-Hennessy Scholars Program. We thank Leng et al. [11] for providing patient MRI data.

References

[1] Wu, S., Chai, A., Arimie, S., Mehra, A., Clavijo, L., Matthews, R. V., and Shavelle, D. M., 2018, "Incidence and Treatment of Severe Primary Mitral Regurgitation in Contemporary Clinical Practice," Cardiovasc. Revascular. Med., **19**(8), pp. 960–963.

[2] Neto, F. L., Marques, L. C., and Aiello, V. D., 2018, "Myxomatous Degeneration of the Mitral Valve," Autopsy Case Rep., **8**(4), p. e2018058.

[3] Timek, T. A., and Miller, D. C., 2001, "Experimental and Clinical Assessment of Mitral Annular Area and Dynamics: What Are we Actually Measuring?," Ann. Thorac. Surg., **72**(3), pp. 966–974.

[4] Levine, R. A., Handschumacher, M. D., Sanfilippo, A., Hagege, A., Harrigan, P., Marshall, J., and Weyman, A., 1989, "Three-Dimensional Echocardiographic Reconstruction of the Mitral Valve, With Implications for the Diagnosis of Mitral Valve Prolapse," Circulation, **80**(3), pp. 589–598.

[5] Salgo, I. S., Gorman, J. H., Gorman, R. C., Jackson, B. M., Bowen, F. W., Plappert, T., St John Sutton, M. G., and Edmunds, L. H., 2002, "Effect of Annular Shape on Leaflet Curvature in Reducing Mitral Leaflet Stress," Circulation, **106**(6), pp. 711–717.

[6] David, T. E., Komeda, M., Pollick, C., and Burns, R. J., 1989, "Mitral Valve Annuloplasty: The Effect of the Type on Left Ventricular Function," Ann. Thorac. Surg., **47**(4), pp. 524–528.

[7] Rausch, M. K., Bothe, W., Kvitting, J.-P. E., Swanson, J. C., Miller, D. C., and Kuhl, E., 2012, "Mitral Valve Annuloplasty," Ann. Biomed. Eng., **40**(3), pp. 750–761.

[8] Frishman, S., Kight, A., Pirozzi, I., Imbrie-Moore, A. M., Paulsen, M. J., Woo, J. Y., and Cutkosky, M. R., 2020, "Selectively Compliant Annuloplasty Ring to Enable Annular Dynamics in Mitral Valve Repair Evaluated by In-Vitro Stereovision," ASME Paper No. DMD2020-9034.

[9] Pitsis, A., Kelpis, T., Theofilogiannakos, E., Tsotsolis, N., Boudoulas, H., and Boudoulas, K. D., 2019, "Mitral Valve Repair: Moving Towards a Personalized Ring," J. Cardiothorac. Surg., **14**(1), pp. 1–7.

[10] Pouch, A. M., Vergnat, M., McGarvey, J. R., Ferrari, G., Jackson, B. M., Sehgal, C. M., Yushkevich, P. A., Gorman, R. C., and Gorman, J. H., III, 2014, "Statistical Assessment of Normal Mitral Annular Geometry Using Automated Three-Dimensional Echocardiographic Analysis," Ann. Thorac. Surg., **97**(1), pp. 71–77.

[11] Leng, S., Zhang, S., Jiang, M., Zhao, X., Wu, R., Allen, J., He, B., San Tan, R., and Zhong, L., 2018, "Imaging 4D Morphology and Dynamics of Mitral Annulus in Humans Using Cardiac Cine MR Feature Tracking," Sci. Rep., **8**(1), p. 81.

[12] Sündermann, S. H., Gessat, M., Cesarovic, N., Frauenfelder, T., Biaggi, P., Bettex, D., Falk, V., and Jacobs, S., 2013, "Implantation of Personalized, Biocompatible Mitral Annuloplasty Rings: Feasibility Study in an Animal Model," Interact. Cardiovasc. Thorac. Surg., **16**(4), pp. 417–422.

[13] Purser, M. F., Richards, A. L., Cook, R. C., Osborne, J. A., Cormier, D. R., and Buckner, G. D., 2011, "A Novel Shape Memory Alloy Annuloplasty Ring for Minimally Invasive Surgery: Design, Fabrication, and Evaluation," Ann. Biomed. Eng., **39**(1), pp. 367–377.
[14] Tjørnild, M. J., Skov, S. N., Røpcke, D. M., Ilkjær, C., Rasmussen, J., Couetil, J.-P., and Nielsen, S. L., 2019, "Mitral Annuloplasty Ring With Selective Flexibility for Septal–Lateral Contraction and Remodelling Properties," Interact. Cardiovasc. Thorac. Surg., **28**(1), pp. 65–70.
[15] Pierce, E. L., Bloodworth, IV, C. H., Siefert, A. W., Easley, T. F., Takayama, T., Kawamura, T., Gorman, R. C., Gorman, III, J. H., and Yoganathan, A. P., 2018, "Mitral Annuloplasty Ring Suture Forces: Impact of Surgeon, Ring, and Use Conditions," J. Thorac. Cardiovasc. Surg., **155**(1), pp. 131–139.
[16] Ncho, B. E., Pierce, E. L., Bloodworth, IV., C. H., Imai, A., Okamoto, K., Saito, Y., Gorman, R. C., Gorman, III, J. H., and Yoganathan, A. P., 2020, "Optimized Mitral Annuloplasty Ring Design Reduces Loading in the Posterior Annulus," J. Thorac. Cardiovasc. Surg., **159**(5), pp. 1766–1774.
[17] Silbiger, J. J., 2012, "Anatomy, Mechanics, and Pathophysiology of the Mitral Annulus," Am. Heart J., **164**(2), pp. 163–176.
[18] Gunning, G. M., and Murphy, B. P., 2014, "Determination of the Tensile Mechanical Properties of the Segmented Mitral Valve Annulus," J. Biomech., **47**(2), pp. 334–340.
[19] Gilbert, H. B., and Webster, R. J., III, 2016, "Rapid, Reliable Shape Setting of Superelastic Nitinol for Prototyping Robots," IEEE Robot. Autom. Lett., **1**(1), pp. 98–105.
[20] Dagum, P., Timek, T., Green, G. R., Daughters, G. T., Liang, D., Ingels, N. B., Jr., and Miller, D. C., 2001, "Three-Dimensional Geometric Comparison of Partial and Complete Flexible Mitral Annuloplasty Rings," J. Thorac. Cardiovasc. Surg., **122**(4), pp. 665–673.
[21] Kong, F., Pham, T., Martin, C., Elefteriades, J., McKay, R., Primiano, C., and Sun, W., 2018, "Finite Element Analysis of Annuloplasty and Papillary Muscle Relocation on a Patient-Specific Mitral Regurgitation Model," PLoS One, **13**(6), p. e0198331.
[22] Serafini, D. B., 1999, "A Framework for Managing Models in Nonlinear Optimization of Computationally Expensive Functions," Ph.D. thesis, Rice University, Houston, TX.
[23] Kochenderfer, M. J., and Wheeler, T. A., 2019, *Algorithms for Optimization*, MIT Press, Cambridge, MA.
[24] Bertil, M., 1986, *Spatial Variation*, Springer-Verlag, New York.
[25] Jones, D. R., Schonlau, M., and Welch, W. J., 1998, "Efficient Global Optimization of Expensive Black-Box Functions," J. Global Optim., **13**(4), pp. 455–492.
[26] Grewal, J., Suri, R., Mankad, S., Tanaka, A., Mahoney, D. W., Schaff, H. V., Miller, F. A., and Enriquez-Sarano, M., 2010, "Mitral Annular Dynamics in Myxomatous Valve Disease: New Insights With Real-Time 3-Dimensional Echocardiography," Circulation, **121**(12), pp. 1423–1431.
[27] Wan, S., Lee, A. P., Jin, C.-N., Wong, R. H., Chan, H. H., Ng, C. S., Wan, I. Y., and Underwood, M. J., 2015, "The Choice of Mitral Annuloplastic Ring–Beyond 'Surgeon's Preference," Ann. Cardiothorac. Surg., **4**(3), p. 261.
[28] Paulsen, M. J., Bae, J. H., Imbrie-Moore, A. M., Wang, H., Hironaka, C. E., Farry, J. M., Lucian, H., Thakore, A. D., Cutkosky, M. R., and Joseph Woo, Y., 2020, "Development and Ex Vivo Validation of Novel Force-Sensing Neochordae for Measuring Chordae Tendineae Tension in the Mitral Valve Apparatus Using Optical Fibers With Embedded Bragg Gratings," ASME J. Biomech. Eng., **142**(1), p. 014501.
[29] Imbrie-Moore, A. M., Paulsen, M. J., Zhu, Y., Wang, H., Lucian, H. J., Farry, J. M., MacArthur, J. W., Ma, M., and Woo, Y. J., 2021, "A Novel Cross-Species Model of Barlow's Disease to Biomechanically Analyze Repair Techniques in an Ex Vivo Left Heart Simulator," J. Thorac. Cardiovasc. Surg., **161**(5), pp. 1776–1783.
[30] Akca, D., 2003, "Generalized Procrustes Analysis and Its Applications in Photogrammetry," ETH, Zurich, Switzerland.
[31] Hedrick, T. L., 2008, "Software Techniques for Two-and Three-Dimensional Kinematic Measurements of Biological and Biomimetic Systems," Bioinspiration Biomimetics, **3**(3), p. 034001.
[32] Wang, H., Paulsen, M. J., Imbrie-Moore, A. M., Tada, Y., Bergamasco, H., Baker, S. W., Shudo, Y., Ma, M., and Woo, J. Y., 2020, "In Vivo Validation of Restored Chordal Biomechanics After Mitral Ring Annuloplasty in a Rare Ovine Case of Natural Chronic Functional Mitral Regurgitation," J. Cardiovasc. Dev. Disease, **7**(2), p. 17.
[33] Kaiser, A. D., McQueen, D. M., and Peskin, C. S., 2019, "Modeling the Mitral Valve," Int. J. Numer. Methods Biomed. Eng., **35**(11), p. e3240.
[34] Garcia, J., Yang, Z., Mongrain, R., Leask, R. L., and Lachapelle, K., 2018, "3D Printing Materials and Their Use in Medical Education: A Review of Current Technology and Trends for the Future," BMJ Simul. Technol. Enhanced Learn., **4**(1), pp. 27–40.
[35] Imbrie-Moore, A. M., Paullin, C. C., Paulsen, M. J., Grady, F., Wang, H., Hironaka, C. E., Farry, J. M., Lucian, H. J., and Woo, Y. J., 2020, "A Novel 3D-Printed Preferential Posterior Mitral Annular Dilation Device Delineates Regurgitation Onset Threshold in an Ex Vivo Heart Simulator," Med. Eng. Phys., **77**, pp. 10–18.
[36] Granegger, M., Aigner, P., Kitzmüller, E., Stoiber, M., Moscato, F., Michel-Behnke, I., and Schima, H., 2016, "A Passive Beating Heart Setup for Interventional Cardiology Training," Curr. Direct. Biomed. Eng., **2**(1), pp. 735–739.
[37] Leopaldi, A. M., Wrobel, K., Speziali, G., van Tuijl, S., Drasutiene, A., and Chitwood, W. R., Jr, 2018, "The Dynamic Cardiac Biosimulator: A Method for Training Physicians in Beating-Heart Mitral Valve Repair Procedures," J. Thorac. Cardiovasc. Surg., **155**(1), pp. 147–155.